International Journal of Thermophysics (2024) 45:47
https://doi.org/10.1007/s10765-024-03335-1

Thermal Properties of NaF–KF and NaF–KF–MgF_2 Molten eutectic Mixtures: Experiment and Simulation

A. V. Rudenko[1] · A. A. Redkin[1] · A. Y. Galashev[1] · K. A. Abramova[1] · O. R. Rakhmanova[1] · E. A. Il'ina[1] · S. V. Pershina[1] · Yu. P. Zaikov[1]

Received: 29 December 2023 / Accepted: 22 January 2024

Abstract
Molten fluoride salts are under development for use as fuel coolant and thermal storage in industrial nuclear energy production. This study focuses on the experimental and molecular dynamic investigation of thermal conductivity and ion diffusion in the eutectic molten salts of NaF–KF and NaF–KF–MgF_2. Experimental and calculated data demonstrate that the temperature-dependent thermal conductivity can be accurately represented as a decaying linear function for both melts. The significant diffusion coefficient of fluorine ions in the NaF–KF molten system can be attributed to the considerable number of Coulomb repulsions among the abundant negative ions in the irregular system. The findings of this study provide insights into the behavior of NaF–KF and NaF–KF–MgF_2 molten salt mixtures under operating conditions in high-temperature power plants.

Keywords Diffusion coefficient · Molten fluoride salts · Molecular dynamics simulation · Laser flash method · Thermal conductivity · Thermal diffusivity

1 Introduction

Molten salts are utilized as coolants and working media that directly contain nuclear fuel in molten salt reactors (MSRs). MSRs can be classified into two types. The first type is a high-temperature fluoride reactor that utilizes molten salts as coolants for heat removal from solid fuel. In the second type of reactor, molten salts are employed to dissolve fuel, facilitating the transformation of chemical elements in nuclear reaction within the molten salt medium. Molten salts are favored for their superior heat transfer properties, low vapor pressures, and minimal reactivity with

✉ O. R. Rakhmanova
oksana_rahmanova@mail.ru

[1] Institute of High Temperature Electrochemistry, Ural Branch of the Russian Academy of Sciences, Akademicheskaya Str., Yekaterinburg, Russian Federation 20620066

Published online: 24 February 2024

air and water. Due to fluorine's lower thermal neutron cross section compared to other halides, fluoride salts are considered to be the perfect ones for the thermal spectrum of MSR. The utilization of molten salt mixtures instead of pure salts allows for a lower melting temperature of the system, enabling a reduction in the operating temperature of the MSR. Thermal conductivity, thermal diffusivity, and ion diffusion, which influence the viscosity of molten salts, are significant kinetic properties for the design of nuclear power systems. Moreover, molten salts find application in high-temperature power generation, such as thermal energy storage systems, concentrating solar power plants, fusion reactors, and various industrial manufacturing processes. High-temperature liquids, including molten salts, employed in nuclear reactors, offer potential improvements in efficiency, safety, and reduced capital costs compared to existing water reactors [1]. However, limited data on the thermophysical properties of numerous candidate salts exist due to challenges associated with measuring these properties at sufficiently high temperatures (e.g., 720–1100 K) [2].

In MSR, fissile fluorides (e.g., UF_4, PuF_3, and ThF_4) are present in the FLiNaK (46.5 LiF–11.5 NaF–42 KF mol %) and FLiBe (66 LiF-34 BeF_2 mol %) molten salts. Hydrodynamic calculations have demonstrated that viscosity and thermal conductivity play a crucial role in heat transfer when FLiNaK is utilized as the working fluid in MSR [3]. The thermal conductivity (λ) of the FLiNaK molten fluoride salt of eutectic composition was measured using the laser flash method within the temperature range of 773–973 K [4]. A linear increase in the λ(T) dependence was observed, while the calculation of the thermal conductivity of FLiNaK across a wider temperature range using an empirical equation yielded a constant value of $\lambda = 0.85$ W/(m K) with a probable deviation of 0.206 W/(m K) [5]. It should be noted that the estimated behavior of λ(T) provided in [5] serves solely as an approximate guideline for practical use and cannot be regarded as an accurate prediction. The presence of a highly light and non-polarizable lithium ion in FLiNaK results in overestimated calculated values of thermal conductivity when determined using the Green–Kubo formula [6]. In contrast to the trend observed in the λ(T) function in [4], both calculated and experimental data indicate a decrease in thermal conductivity with rising temperature within the range of 750–1300 K [6]. Through equilibrium molecular dynamics (MD) calculations, a linear decrease in the λ(T) dependence of FLiNaK thermal conductivity was observed at temperatures of 950 K, 1100 K, and 1250 K [7]. Additionally, Rudenko et al. [8] obtained thermal diffusivity using the laser flash method and measured heat capacity through the Differential Scanning Calorimetry (DSC) method, with all these results exhibiting relatively close values. Within the temperature range of 723–873 K, the thermal conductivity value varies from 0.7 to 0.8 W/m K.

A weak negative dependence of thermal conductivity on temperature was observed through equilibrium MD simulation in the microcanonical ensemble for molten NaCl and KCl [9]. Ishii et al. [10] employed the MD method with potentials incorporating the polarization of ions to establish the dependencies of λ on the density of the system for both pure liquid LiF (KF) and their molten equimolecular mixture LiF–KF. In all cases, a linear increase in the coefficient λ was observed with an increase in the system's density. The work extensively discusses the factors influencing the heat transfer process in molten systems; however, experimental data

for the simulated systems are not provided. The thermal conductivity of the molten NaF–KF eutectic mixture was investigated by Smirnov et al. [11] within the temperature range of 1160–1250 K. According to the temperature dependence equation, λ was determined to be 0.63 W/m K near the melting point.

Recently, an experimental study on the thermal conductivity of the NaF–KF–MgF_2 (34.5–59.0–6.5 mol%) molten salt mixture was conducted using a needle probe within a narrow temperature range of 900–1100 K [12]. The data obtained exhibited a relatively significant temperature dependence of the λ coefficient. Similarly, for the FLiNaK and LiCl–KCl systems, a negative slope of the linear fitting for λ(T) was observed.

Therefore, it can be noted that today there is uncertainty in measuring the thermal conductivity of halide melts. Experimental determination is complicated by the presence of high temperatures in such systems and the presence of aggressive and radioactive additives. In turn, theoretical models have a number of limitations associated with the method applied [13, 14]. Therefore, for matters concerning heat transfer in salt systems, it is necessary to develop an integrated approach that combines experimental and theoretical methods. This approach will not only serve to validate the obtained data from both modeling and experiment but also contribute to a deeper understanding of heat transfer mechanisms in high-temperature molten systems.

The objective of this research is to experimentally determine the kinetic properties of NaF–KF and NaF–KF–MgF2 molten salts, as well as the qualitative and quantitative verification of the obtained dependencies within the developed molecular dynamics model.

2 Materials and Methods

2.1 Laser Flash Method

Thermal diffusivity was determined using an original technique specifically designed for molten media [15–17]. A small sample of the salt mixture was placed in a dedicated cell made of NP2 alloy and melted here and covered by metallic cap. After cooling the cap was welded to cell and the cell was covered by graphite. By employing this approach, the potential influence of graphite spray on the salt sample and its impact on melt properties were eliminated. Notably, our results for molten FLiNaK [8] exhibit agreement within 5% with data obtained through other measurement techniques.

The cell was then positioned within a holder inside a high-temperature electric furnace. For every molten salt sample two runs (Run I, Run II) were executed for statistics. Throughout the high-temperature measurements, it was observed that the NP2 alloy maintained a vibrant metallic luster and did not darken, even after extensive long-duration experiments. To enhance the blackness of the surfaces, the sample cell was treated with emery paper and coated with a thin layer (~5 μm) of graphite spray. After the experiment, the graphite layer could be easily removed using alcohol, and there was no interaction between the NP2 material and carbon. The

shape of the cell remained unaltered following the high-temperature experiments. Further details of the precise experimental technique can be found in [8].

2.2 Heat Capacity Measurements

The heat capacity was studied using a STA 449F1 Jupiter synchronous thermal analyzer (NETZSCH, Germany). This device enables simultaneous recording of both the sample mass changes and the Differential Scanning Calorimetry (DSC) curve. The experimental equipment ensures precise measurement accuracy for the specified parameters: temperature (±1.5 K), mass (< 10–6 g), baseline reproducibility (±2.5 mW), and enthalpy (±3%). Further information regarding the experimental technique can be found in our previous paper [18].

2.3 Sample Preparation

To prepare the FMgNaK (NaF–KF–MgF_2) and NaF–KF molten salt mixtures, the following components were used: commercial extra pure magnesium fluoride (JSC REAHIM Ltd., Moscow, Russia); commercial extra pure sodium fluoride NaF (JSC Halogen, Perm, Russia); and commercial extra pure potassium hydrofluoride KF·HF (JSC REAHIM Ltd., Moscow, Russia). Each container with KF·HF was analyzed according to GOST 10067-80 for the HF content, which averaged 25.84 ± 0.07 wt%. The starting components were melted in ambient air using a glassy carbon crucible positioned within a protective alundum vessel. Graphite chips were inserted between the crucibles to prevent the glassy carbon from burning. The KF component, known for its high hygroscopicity, was added in the form of KF·HF, which decomposes into KF and HF within the temperature range of 673–773 K. This decomposition process fluorinates the oxygen-containing impurities (Table 1).

During melting of the initial components in ambient air, the resistance furnace was incrementally heated as follows: 1) initially, the temperature was raised to 673 K and held for 120 min. This step aimed to eliminate any moisture present and initiate

Table 1 Summary of sample descriptions

Chemical Name	Formula	Source	Purity according to supplier, %
Eutectic mixture NaF–KF	NaF–KF	Prepared here	99.0*
Sodium fluoride	NaF	Vekton	99.8[a]
Potassium bifluoride	KF·HF	Vekton	99.5[a]
Magnesium fluoride	MgF_2	JSC REAHIM	99.99[a]
Argon	Ar	Uralkriogas	99.993[b]
Eutectic mixture NaF–KF–MgF_2	NaF–KF–MgF_2	Prepared here	99.0*

[a]Mass fraction purity

[b]Mole fraction purity

*Purity according to chemical analysis

the decomposition of KF·HF, resulting in the release of HF; 2) subsequently, the temperature was further increased from 673 to 773 K and maintained for 120 min. During this phase, the majority of the HF was decomposed, and the salt mixture began to melt. Once the temperature of 773 K was attained, the melt was stirred to eliminate HF from the crucible walls; and (3) the temperature was increased from 773 K to 973–993 K and maintained for 60 min. Following this, the temperature was held steady at 973–993 K for 90 min, continuing the periodic stirring with the glassy carbon rod. This process ensured the removal of all remaining HF from the melt. The crucible containing the prepared molten salt was removed from the furnace and allowed to cool in ambient air until reaching a temperature of 623 K. Subsequently, it was transferred to a glove-box filled with an inert argon atmosphere, where the salt further cooled under vacuum conditions. Once the melt was fully cooled, it was weighed and sampled for chemical analysis within the glove-box. The solidified salt was then milled for subsequent utilization.

Following solidification, the individual sample pieces weighed approximately 0.4–0.7 g. In order to achieve a total weight close to 1.5 g, several samples were placed in a nickel container and then heated in a furnace above the melting point. During this process, the absence of gas bubbles at the bottom of the container was visually monitored. If any gas bubbles were present, they were eliminated by mechanically stirring the melt with a nickel wire. Following the heating process, the container was removed from the furnace and promptly sealed with a lid while still hot. The entire container assembly was then reheated to a temperature above the melting point. Once cooled, the samples were extracted from the glove-box in a tightly sealed container and removed from the container just prior to welding.

Following welding using an argon-arc apparatus, the samples were put again into the glove-box and heated above the melting point. Subsequently, they were cooled, labeled, and packaged into containers. After preparation, the samples were subjected to the thermal analysis using the DSC method. The results obtained are presented in Figs. 1 and 2. The NaF–KF mixture exhibited a melting point of 989 K, while the FMgNaK mixture had a melting point of 960 K, which corresponds to literature data [19, 20].

2.4 Molecular Dynamics Simulation Model

Computer simulation methods are commonly employed to refine experimental data and evaluate scientific hypotheses. In the study of complex chemical systems like high-temperature molten salts, the molecular dynamics (MD) method is traditionally used [21]. With this method, it becomes possible to investigate substance structures [22], obtain qualitative and quantitative results through modeling physicochemical processes, and determine their properties with accuracy [7, 23].

In order to simulate the NaF–KF eutectic molten salt, an MD model was constructed with a total of 3750 atoms. The ratio of components in the model corresponded to the experimental data, with 40-mol% NaF (1500 atoms) and 60-mol% KF (2250 atoms).

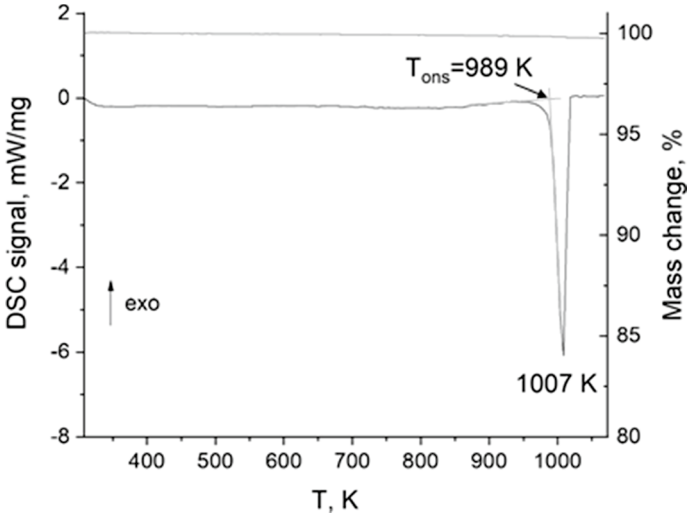

Fig. 1 Thermal analysis of NaF–KF by DSC

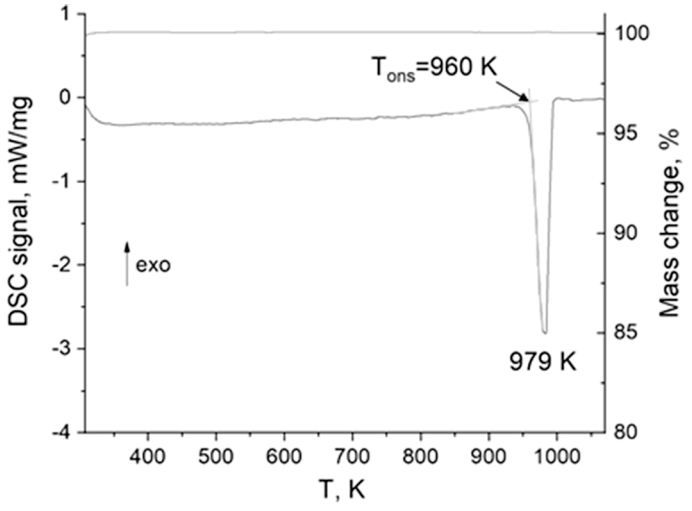

Fig. 2 Thermal analysis of NaF–KF–MgF_2 by DSC

Two crystals were positioned in the rectangular simulation cell, each with a face-centered cubic lattice. The lattice parameter used for NaF was a = 0.46344 nm and for KF, a = 0.534 nm. Figure 3a provides an overview of the system at the initial time moment (t = 0 ps), illustrating the geometric dimensions of the simulation cell. Prior to the main MD calculation, a geometric optimization of the system was performed. Subsequently, the system was heated to a temperature of 1300 K and maintained at this temperature for 1.2 ns within the NVT ensemble [24]. Subsequently, the system was cooled down to

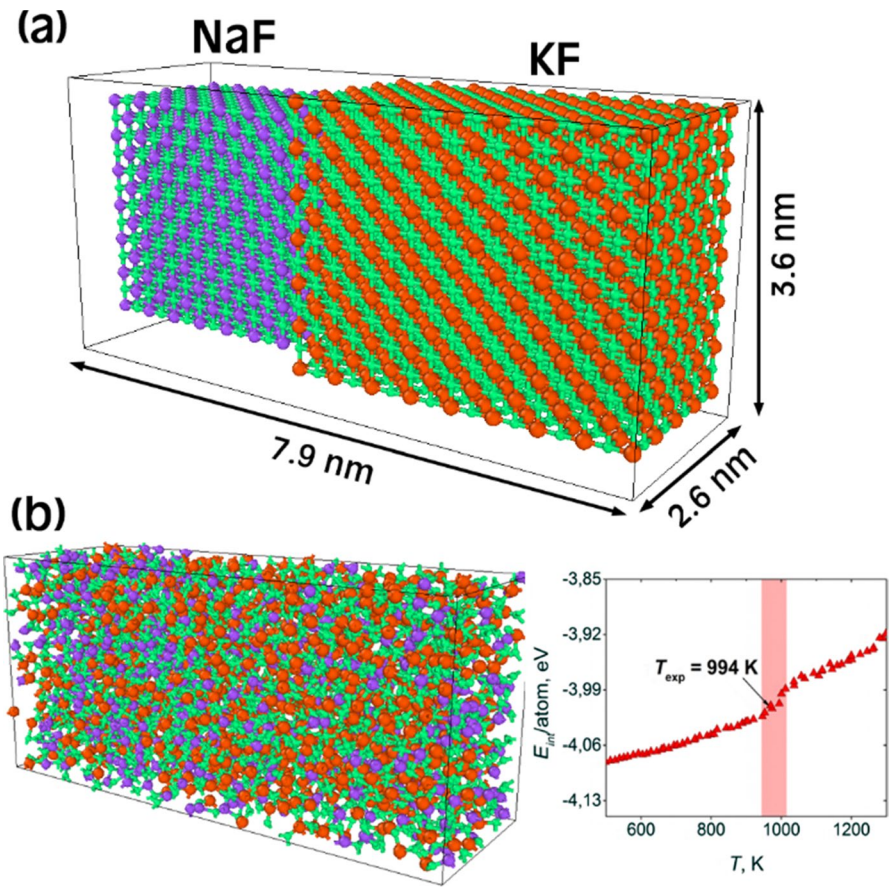

Fig. 3 **a** General view of the 40-mol% NaF–60-mol% KF system at the initial time moment of the simulation; **b** well-mixed molten system of Na^+, K^+, F^- ions at the operating temperature (1123 K); the inset graph depicts a curve describing the change in the specific internal energy E_{int}/atom of the system with temperature, and the melting range of 950–1010 K is highlighted by the red color

the operating temperature (998, 1023, 1048, 1073, 1098, and 1123 K) over a period of 1 ns under the NPT ensemble. Figure 3b illustrates a well-mixed system after relaxation at the operating temperature, specifically at 2.2 ns. The inset graph depicts the temperature dependence of the internal energy per atom (E_{int}/atom), with the red region representing the calculated range for the melting temperature of the system (950–1010 K). It is worth noting that the experimental liquidus temperature for the considered system was determined to be 994 K [19]. Once the system reached a state of complete equilibrium, the thermal conductivity calculation was performed using the Green–Kubo method within the NVE ensemble. To maintain a constant simulated temperature, the Nose–Hoover thermostat was employed. Periodic boundary conditions were applied

throughout the calculations. Long-range interactions were handled using the PPPM (a Particle–Particle Particle–Mesh) summation method. The Verlet algorithm was used to solve Newton's equations of motion with a time step of $\Delta t = 10^{-15}$ s [25]. In order to simulate the interatomic interactions within the NaF–KF molten system, the Born–Huggins–Mayer potential was employed, with the parameters specified in [25].

The diffusion coefficients of the individual components of the investigated molten salt depending on the temperature were calculated in the model using the Einstein relation through the slope to the time axis of the mean square displacement Δr^2 of the center of mass of similar atoms:

$$D = \lim_{t\to\infty} \frac{1}{2t}[\Delta \boldsymbol{r}(t)]^2. \tag{1}$$

2.5 Thermal Conductivity Calculation

In the MD model, the thermal conductivity λ of the molten salt can be calculated using the equilibrium Green–Kubo formalism through the auto-correlation function of the heat flux $\boldsymbol{J}$

$$\lambda = \frac{V}{3k_B T^2} \int_0^\infty \boldsymbol{J}(0) \cdot \boldsymbol{J}(t) dt, \tag{2}$$

where V is the volume of the simulation cell, k_B is the Boltzmann constant, and T is the calculation temperature.

The heat flux is defined through the per-atom stress tensor $\boldsymbol{S}_i$ as

$$\begin{aligned} \mathbf{J} &= \frac{1}{V}\left[\sum_i e_i \mathbf{v}_i - \sum_i \mathbf{S}_i \mathbf{v}_i\right] = \frac{1}{V}\left[\sum_i e_i \mathbf{v}_i + \sum_{i<j} (\mathbf{F}_{ij} \cdot \mathbf{v}_j)\mathbf{r}_{ij}\right] = \\ &= \frac{1}{V}\left[\sum_i e_i \mathbf{v}_i + \frac{1}{2}\sum_{i<j} (\mathbf{F}_{ij} \cdot (\mathbf{v}_i + \mathbf{v}_j))\mathbf{r}_{ij}\right], \end{aligned} \tag{3}$$

where e_i is the per-atom energy (potential and kinetic), $\mathbf{v}_i$, $\mathbf{v}_j$ are the 3×3 velocity matrix vectors of i and j particles, $\boldsymbol{F}_{ij}$ is the force acting between i and j particles, and $\boldsymbol{r}_{ij}$ is the distance between i and j ions in the molten salt [10].

All calculations were performed using the open-source program code for MD simulation LAMMPS [26] on the URAN cluster-type hybrid computer at the N.N. Krasovskii Institute of Mathematics and Mechanics UB RAS.

3 Results

3.1 Heat Capacity

The obtained data of heat capacity for the melts under investigation together with standard uncertainties are summarized in Table 2.

Table 2 Heat capacity (C_p) for (60 ± 1 mol%) KF–(40 ± 1 mol% NaF) and NaF–KF–MgF_2 at pressure p = 0.1 MPa

NaF–KF		NaF–KF–MgF_2	
T, K	C_p, J g^{-1} K^{-1}	T, K	C_p, J g^{-1} K^{-1}
1003	1.35	994	1.37
1008	1.38	999	1.36
1013	1.35	1004	1.37
1018	1.36	1009	1.34
1023	1.39	1014	1.33
1028	1.39	1019	1.32
1033	1.4	1024	1.37
1038	1.38	1029	1.37
1043	1.38	1034	1.39
		1039	1.39
		1044	1.4

[a]Standard uncertainties u are $u(C_p) = 0.04$ J g^{-1} K^{-1} and $u(T) = 1.5$ K

4 Thermal Diffusivity

4.1 Eutectic Mixture NaF–KF

Thermal diffusivity α of the NaF–KF eutectic mixture (0.6KF-0.4NaF) was measured at temperatures above the melting point. The results obtained are presented in Table 3 and Fig. 4.

Thermal diffusivity values α range from 0.2 to 0.3 cm^2/s in the molten state. To determine the thermal conductivity λ, knowledge of the density ρ and heat capacity C_p

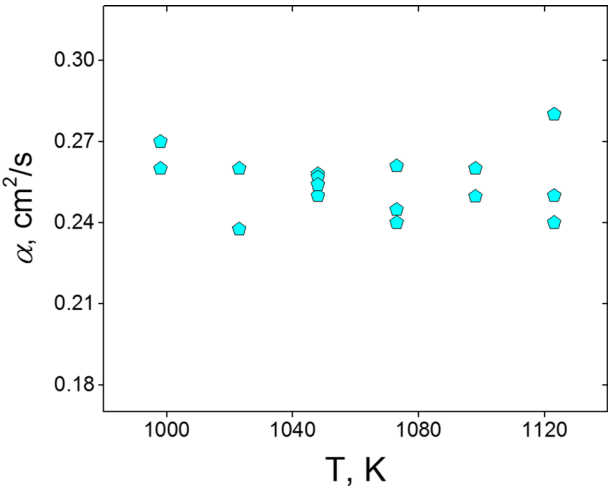

Fig. 4 Thermal diffusivity of the molten KF–NaF mixture

Table 3 Thermal diffusivity (α), density (ρ), heat capacity (C_p), and thermal conductivity (λ) for (60 ± 1 mol%) KF–(40 ± 1 mol% NaF) mixture at pressure p = 0.1 MPa

T, K	α, cm^2/s	C_p, J/g•K	ρ, g/cm^3	λ, W/m•K
Run I 1123	0.240	1.38	1.90	0.63
1098	0.250	1.38	1.91	0.66
1073	0.245	1.38	1.93	0.65
1048	0.258	1.38	1.94	0.69
1023	0.260	1.38	1.96	0.70
998	0.260	1.38	1.97	0.71
Run II 1123	0.250	1.38	1.90	0.65
1098	0.260	1.38	1.91	0.69
1073	0.261	1.38	1.93	0.69
1048	0.257	1.38	1.94	0.69
1023	0.238	1.38	1.96	0.64
998	0.270	1.38	1.97	0.73

Standard uncertainties u are $u(\alpha) = 0.02$ mm^2s^{-1}, $u(\rho) = 0.014$ g cm^{-3}, $u(C_p) = 0.04$ J g^{-1} K^{-1}, $u(\lambda) = 0.04$ W m^{-1} K^{-1}, and $u(T) = 0.5$ K

values is required. The heat capacity was measured experimentally, while the density was referenced from the Janz handbook [27]. The obtained results for the calculated thermal conductivity λ values are presented in Table 1. The thermal diffusivity α of molten NaF–KF is comparable to that of FLiNaK. However, the thermal conductivity λ is lower in NaF–KF system due to its lower heat capacity.

4.2 Eutectic Mixture NaF–KF–MgF_2

Thermal diffusivity α of the NaF–KF–MgF_2 eutectic mixture was measured at temperatures exceeding the melting point. The thermal properties are shown in Table 4, and the temperature dependence of thermal diffusivity $\alpha(T)$ is illustrated in Fig. 5.

Standard uncertainties u are $u(\alpha) = 0.02$ mm^2s^{-1}, $u(\rho) = 0.014$ g cm^{-3}, $u(C_p) = 0.04$ J g^{-1} K^{-1}, $u(\lambda) = 0.04$ W m^{-1} K^{-1}, and $u(T) = 0.5$ K.

Thermal diffusivity of the NaF–KF–MgF_2 eutectic mixture varies from 0.255 to 0.275 cm^2/s within the temperature range of 990–1060 K. The density values, as shown in Table 4, were obtained from [28]. Thermal conductivity was observed to decrease with temperature as depicted in Fig. 6. However, our findings indicate a more moderate decline in thermal conductivity compared to the results reported by Merrit et al. [12]. The predictive values of thermal conductivity by Yang et al. are also shown in Fig. 6 [29].

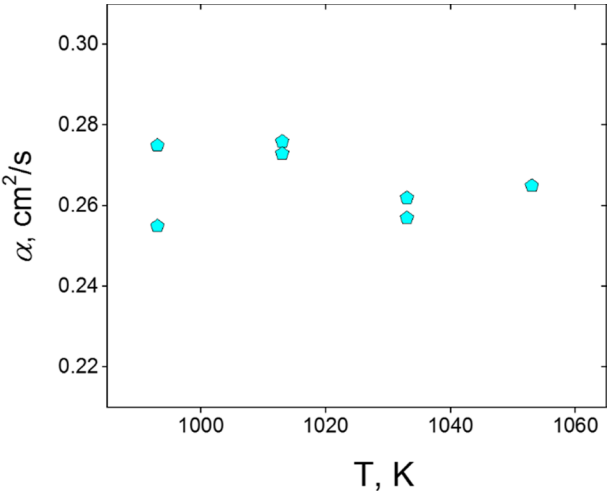

Fig. 5 Thermal diffusivity of the molten NaF–KF–MgF_2

Table 4 Thermal diffusivity (α), density (ρ), heat capacity (C_p), and thermal conductivity (λ) for (59.0 mol%±1 mol%) KF–(34.5±1 mol% NaF)–(6.5±1 mol% MgF2) mixture at pressure $p = 0.1$ MPa

T, K	α, cm^2/s	C_p, J/g•K	ρ, g/cm^3	λ, W/m•K
Run I 1033	0.262	1.35	2.05	0.72
1013	0.276	1.35	2.06	0.77
993	0.255	1.35	2.07	0.71
Run II 1053	0.265	1.35	2.04	0.73
1033	0.257	1.35	2.05	0.71
1013	0.273	1.35	2.06	0.76
993	0.275	1.35	2.07	0.77

4.3 Computer Simulation Data

The diffusion coefficients of the individual components Na^+, K^+, and F^- in the investigated molten salt NaF–KF are represented in Fig. 7. The F^- ions exhibit the highest diffusion coefficient, reaching a value of $9 \cdot 10^{-5}$ cm^2/s. Additionally, there is a noticeable upward trend in the D(T) dependencies for Na^+ and K^+ ions. The average diffusion coefficient for Na^+ ions is approximately 5% higher than that of K^+ ones.

Figure 8 presents the thermal conductivity values obtained from our experimental measurements (blue circles) and the MD simulation (red diamonds). The figure also includes the linear fitting of the obtained results (solid and dashed lines), as well as analytical dependencies for λ(T). Both the experimental and simulated data exhibit a

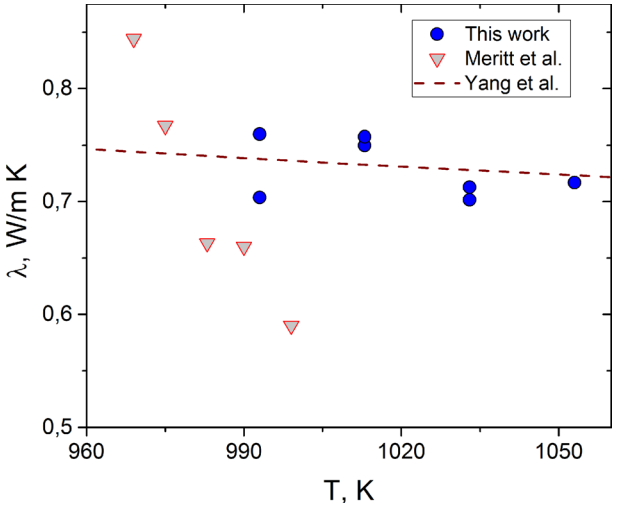

Fig. 6 Thermal conductivity of the molten KF–NaF–MgF_2 mixture

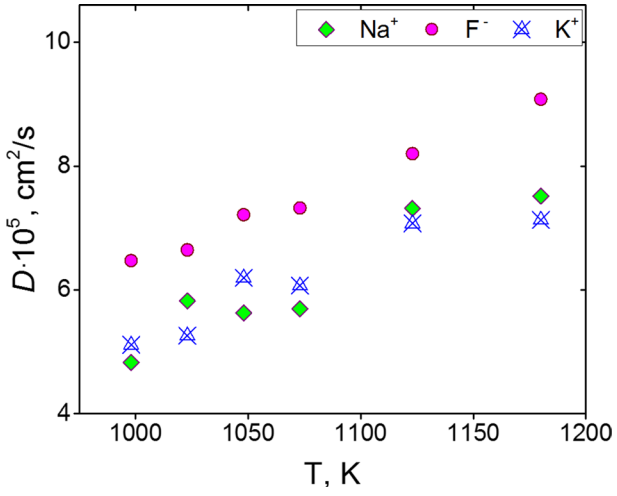

Fig. 7 The temperature dependence of the diffusion coefficients for the components of the 40-mol% NaF–60-mol% KF molten system obtained through the MD model

decreasing trend with increasing temperature. The values obtained in the MD model were found to be slightly higher than the experimental data, but the discrepancy did not

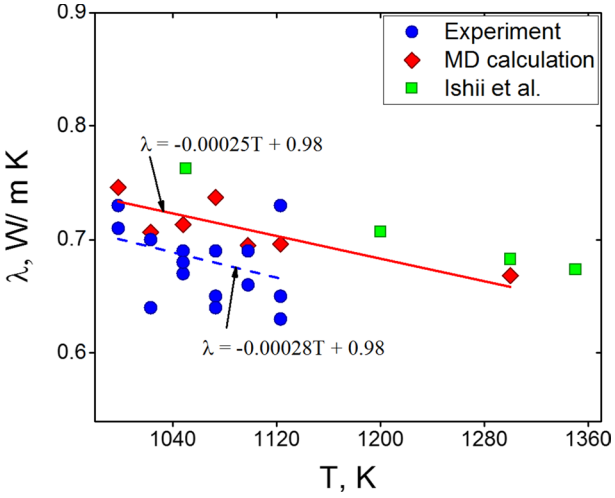

Fig. 8 Thermal conductivity of the 40-mol% NaF–60-mol% KF molten system as a function of temperature; the experimental data are represented by blue circles; the MD data are shown as red diamonds; solid and dashed lines correspond to the linear fitting of the obtained data; the analytical expressions for λ corresponding to the linear approximation are also displayed

exceed 10%. Figure 8 also includes the data obtained in [10], which shows good agreement with the values calculated in this study.

5 Discussion

The thermal diffusivity of fluoride and chlorides mixtures shows similar values with weak dependence on temperature. DiGillio and Teja [30] observed that most of the results on the thermal conductivity of KNO_3 obtained before 1980 exhibited a positive temperature dependence. The negative thermal conductivity temperature coefficient was obtained by Nagasaka for molten halides [31–33]. And recent investigations have also revealed negative temperature dependencies for fluorides. Currently, there are no established criteria to justify the reliability of thermal conductivity results. However, the majority of theoretical studies have reported negative temperature dependencies [7, 10]. The models proposed by Ohtori [34] derived the negative temperature dependence on density for molten alkali halides.

The influence of magnesium fluoride on the thermal conductivity of alkali fluoride mixtures is highly debated. There is a possibility that the number of particles in a molecule can impact the thermal conductivity values [35]. Therefore, the addition of MgF_2 can potentially increase the thermal conductivity. However, this effect is expected to be significant only at higher concentrations of magnesium fluoride.

Determining the thermophysical properties of binary and ternary molten salt systems is challenging due to the high temperature required for experiments and the complexity arising from the interaction between high-temperature molten salts and construction materials. Furthermore, conducting such experiments incurs significant

costs. However, knowledge of thermophysical properties is crucial for accurate and optimal technological design. In many ways, these difficulties can be overcome with the help of MD simulation. Our MD calculations showed that the thermal conductivity of the NaF–KF molten system exhibits a decaying trend with temperature, which is also confirmed experimentally. Additionally, the difference between the simulated and experimental data is no more than 10%.

Among other fluoride eutectics, the NaF–KF molten system exhibits one of the highest thermal conductivities. The total mass of positively charged ions in the NaF–KF eutectic is 1.7 times greater than that of negatively charged ions. However, this is not the main reason for the significantly higher diffusion coefficient of F^- ions compared to the diffusion coefficients of the positively charged ions (Na^+ and K^+). The Coulomb interaction between ions plays a crucial role in molten salt. In this case, the number of negatively charged F^- ions exceeds both the number of Na^+ and K^+ ions. The absence of local compensation of positive and negative ions in molten salt results in repulsive interactions between ions of the same charge. Due to their different ionic radii, the heavier positive ions experience greater resistance to movement during these collisions compared to the negative ions. Consequently, the diffusion coefficient of F^- ions is high. Similar higher values of the diffusion coefficient of F^- ions compared to the diffusion coefficients of positive ions are also observed in the eutectic FLiNaK melt [36]. Additionally, Na^+ ions are 1.4 times smaller in size compared to K^+ ions and they are 1.7 times lighter. These factors contribute to a slight (5%) advantage in the diffusion of Na^+ ions over K^+ ions in the NaF–KF molten system.

6 Conclusion

In this study, the kinetic characteristics of the NaF–KF and NaF–KF–MgF_2 eutectic molten salts are determined experimentally and using molecular dynamics methods within the operating temperature range of power plants. The results indicate that the temperature dependences of thermal conductivity and diffusion coefficients of the same type of ions in the NaF–KF molten salt can be accurately described by linear dependences. Furthermore, in both cases, the thermal conductivity demonstrates a decreasing trend with rising temperature, while the diffusion coefficients show an increasing trend. The abundance of F^- ions in the NaF–KF melts leads to stronger Coulomb repulsion between them. Consequently, these ions exhibit the highest mobility in the molten salt.

The findings from this study will aid in the evaluation of molten salts as suitable working fluids for high-temperature power plants. Understanding the energy characteristics of molten salts enables improved power plant efficiency and the development of safety measures to ensure their secure operation.

Author Contributions Conceptualization: [AAR] and [AVR]; Data Curation: [AVR]; Formal Analysis: [AVR], [AAR], [KAA], [ORR], [EAI], and [SVP]; Funding Acquisition: [YPZ]; Investigation: [AVR],

[AAR], [KAA], [ORR], [EAI], and [SVP]; Methodology: [EAI] and [SVP]; Project Administration: [YPZ]; Software: [AVR]; Supervision: [AYG] and [YPZ]; Validation: [ORR] and [KAA]; Visualization: [AVR], [KAA], and [ORR]; Writing—Original Draft Preparation: [AAR], [AVR], [AYG], [KAA], and [ORR]; Writing—Review & Editing: [AAR], [AVR], [AYG], [KAA], and [ORR].

Funding The study was funded by the Scientific Research Program of the Government of Russian Federation**,** 122020100205-5 (FUME-2022-0005).

Declarations

Competing interests The authors have no relevant financial or non-financial interests to disclose.

References

1. B. Mignacca, G. Locatelli, Prog. Nucl. Energ. **129**, 103503 (2020). https://doi.org/10.1016/j.pnucene.2020.103503
2. R. Gallagher, C. Agca, N. Russell, J. Mc Murray, N. Bull Fzell, J. Chem. Eng. Data. **67**, 1406 (2022). https://doi.org/10.1021/acs.jced.2c00081
3. R. Freile, M. Kimber, E.P.J. Nucl, Sci. Technol. **5**, 16 (2019). https://doi.org/10.1051/epjn/2019027
4. S. Robertson, R. Wiser, W. Yang, S. Kang et al., J. Appl. Phys. **131**, 225102 (2022). https://doi.org/10.1063/5.0088059
5. R. Serrano-Lopez, J. Fradera, S. Cuesta-López, Chem. Eng. Proc.: Proc. Intensific. **73**, 87 (2013). https://doi.org/10.1016/j.cep.2013.07.008
6. R.C. Gallagher, A. Birri, N.G. Russell, A.-T. Phan, A.E. Gheribi, J. Mol. Liq. **361**, 119151 (2022). https://doi.org/10.1016/j.molliq.2022.119151
7. A. Gheribi, P. Chartrand, J. Chem. Phys. **144**, 084506 (2016). https://doi.org/10.1063/1.4942197
8. A. Rudenko, A. Redkin, E. Il'ina, S. Pershina, P. Mushnikov, Materials. **15**, 5603 (2022). https://doi.org/10.3390/ma15165603
9. N. Galamba, C.A. Nieto de Castro, J. Ely, J. Chem. Phys. **120**, 8676 (2004). https://doi.org/10.1063/1.1691735
10. Y. Ishii, K. Sato, M. Salanne, P. Madden, N. Ohtori, J. Phys. Chem. B **118**, 3385 (2014). https://doi.org/10.1021/jp411781n
11. M. Smirnov, V. Khokhlov, E. Filatov, Electrochim. Acta **32**, 1019 (1987). https://doi.org/10.1016/0013-4686(87)90027-2
12. B. Merritt, M. Seneca, B. Wright, N. Cahill et al., Int. J. Thermophys. **43**, 149 (2022). https://doi.org/10.1007/s10765-022-03073-2
13. B. Mortazavi, E.V. Podryabinkin, I.S. Novikov, T. Rabczuk, X. Zhuang, A.V. Shapeev, Comput. Phys. Commun. **258**, 107583 (2021). https://doi.org/10.1016/j.cpc.2020.107583
14. N. Ohtori, T. Oono, K. Takase, J. Chem. Phys. **130**, 044505 (2009). https://doi.org/10.1063/1.3064588
15. S. Stankus, I. Savchenko, Thermophys. Aeromech. **16**, 585 (2009). https://doi.org/10.1134/S0869864309040076
16. A. Agazhanov, R. Abdullaev, D. Samoshkin, S. Stankus, Russ. J. Phys. Chem. A **95**, 1291 (2021). https://doi.org/10.1134/S0036024421070037
17. A. Redkin, E. Ili'na, S. Pershina, P. Mushnikov et al., Thermo. **2**, 107 (2022). https://doi.org/10.3390/thermo2030010
18. A. Redkin, I. Korzun, T. Yaroslavtseva, O. Reznitskikh, Y. Zaikov, J. Therm. Anal. Calorim.. **128**, 621 (2017). https://doi.org/10.1007/s10973-016-5869-9
19. J. Holm, Acta Chem. Scand. **19**, 638 (1965). https://doi.org/10.3891/acta.chem.scand.19-0638
20. P. Chartand, A.D. Pelton, Metall. Mater. Trans. **32**(6), 1385 (2001). https://doi.org/10.1007/s11661-001-0228-1
21. M.S. Badar, S. Shamsi, J. Ahmed, M.A. Alam. Molecular dynamics simulations: Concept, methods, and applications. In: Rezaei N, editor. Transdisciplinarity. Vol. 5. Switzerland: Springer. 2022. pp. 131–151. https://doi.org/10.1007/978-3-030-94651-7_7

22. A. Galashev, K. Ivanichkina, Chem. Phys. **555**, 111455 (2022). https://doi.org/10.1016/j.chemphys.2022.111455
23. K. Ivanichkina, A. Galashev, A. Isakov, Appl. Surf. Sci. **561**, 149959 (2021). https://doi.org/10.1016/j.apsusc.2021.149959
24. D. Evans, B. Holian, J. Chem. Phys. **84**, 4069 (1985). https://doi.org/10.1063/1.449071
25. A. Galashev, O. Rakhmanova, K. Abramova, K. Katin et al., J. Phys. Chem. B **127**, 1197 (2023). https://doi.org/10.1021/acs.jpcb.2c06915
26. S. Plimpton, J. Comp. Phys. **117**, 1 (1995). https://doi.org/10.1006/jcph.1995.1039
27. G.J. Janz, R.P.T. Tomkins. Physical properties data compilations relevant to energy storage. IV. Molten salts: Data on additional single and multicomponent salt systems. Washington: National Bureau of Standards; 1981.
28. A. Solano, A. Clark, K. Detrick, M. Memmott, S. Nickerson, J. Nucl. Mater. **557**, 153248 (2021). https://doi.org/10.1016/j.jnucmat.2021.153248
29. H. Yang, R.C. Gallagher, A.-T. Phan, P. Chartrand, A. Gheribi, Materialstoday Energy. **38**, 101441 (2023). https://doi.org/10.1016/j.mtener.2023.101441
30. R. Digulio, A. Teja, Int. J. Thermophys. **13**, 855–871 (1992). https://doi.org/10.1007/BF00503912
31. N. Nakazawa, Y. Nagasaka, A. Nagashima, Int. J. Thermophys. **13**, 753 (1992). https://doi.org/10.1007/BF00503904
32. N. Nakazawa, Y. Nagasaka, A. Nagashima, Int. J. Thermophys. **13**, 763 (1992). https://doi.org/10.1007/BF00503905
33. N. Nakazawa, Y. Nagasaka, A. Nagashima, Int. J. Thermophys. **13**, 555 (1992). https://doi.org/10.1007/BF00501941
34. N. Ohtory, T. Oono, K. Takase, J. Chem. Phys. **130**, 044505 (2009). https://doi.org/10.1063/1.3064588
35. A. Redkin, Y. Zaikov, O. Tkacheva, S. Kumkov, Ionics **22**, 143 (2016). https://doi.org/10.1007/s11581-015-1592-y
36. A. Galashev, Nucl. Eng. Technol. **55**, 1324 (2023). https://doi.org/10.1016/j.net.2022.12.029